Band Alignment of Antimony and Bismuth Silver-Bromide Double Perovksites

Seán Kavanagh,[*,†,‡,¶] Daniel W. Davies,[†,¶] Aron Walsh,[‡,§] and David O. Scanlon[†,¶,‖]

†Department of Chemistry, University College London, 20 Gordon Street, London WC1H 0AJ, UK

‡Department of Materials, Imperial College London, Exhibition Road, London SW7 2AZ, UK

¶Thomas Young Centre, University College London, Gower Street, London WC1E 6BT, United Kingdom

§Global E3 Institute and Department of Materials Science and Engineering, Yonsei University, Seoul 120-749, South Korea

‖Diamond Light Source Ltd., Diamond House, Harwell Science and Innovation Campus, Didcot, Oxfordshire OX11 0DE, UK

E-mail: sean.kavanagh.19@ucl.ac.uk

1

Computational Methodology

All calculations were performed using Density Functional Theory (DFT) within periodic boundary conditions through the Vienna Ab Initio Simulation Package (VASP).[1–4] The PBEsol DFT functional was used for geometry optimizations and calculations of static dielectric constants,[5] while the hybrid functional HSE06 was implemented for band structure, band offset and optical calculations,.[6] To fully account for relativistic effects, spin–orbit interactions were included (HSE06+SOC) in all electronic and optical calculations. HSE06 is a range-separated, screened hybrid-DFT functional which incorporates 25% exact Hartree–Fock exchange for short-range interactions, using a screening parameter of $\omega = 0.11\,\mathrm{bohr}^{-1}$, with the remaining exchange-correlation effects treated by the Generalized Gradient Approximation (GGA) DFT functional PBE.[7] Scalar-relativistic pseudopotentials were employed, and the projector-augmented wave method was used to describe the interaction between core and valence electrons.[8] The ionic dielectric response was calculated under Density Functional Perturbation Theory (DFPT),[9] while the optical response was calculated using the method of Furthmüller et al. to obtain the high-frequency real and imaginary dielectric functions.[9] A convergence criterion of $1\,\mathrm{meV/\AA}$ was imposed on the forces on each atom during structural optimization. Bulk electronic structure calculations were carried out using a $5 \times 5 \times 5$ Monkhorst-Pack k-point mesh and a well-converged 550 eV plane-wave cutoff, while a tighter k-mesh of $9 \times 9 \times 9$ was used for the optical calculations. Charge carrier effective masses were obtained from non-parabolic fitting of the electronic band edges using the *effmass* package,[10] and electronic band structure diagrams were generated using the *sumo* package.[11]

In each calculation, convergence with respect to k-point density and plane-wave energy cutoff was confirmed for the property of interest. The equilibrium structures and input calculation parameters, alongside convergence analysis, of the crystal materials investigated in this report are provided in an online repository at: `https://github.com/SMTG-UCL/Bi_Sb_double_perovskites`.

Band Alignment

In order to calculate the relative alignment of the electron bands, the electrostatic potential offset between the two materials, ΔV, was required. This was determined using the method of Butler et al.,[12] with calculated values for ΔV verified by comparison with relative core-level energy shifts. A 160-atom heterojunction supercell of length 89 Å, consisting of eight primitive unit cells each of $Cs_2AgSbBr_6$ and $Cs_2AgBiBr_6$, was generated using the average lattice parameter of the two structures, with no interfacial atomic relaxation permitted. Electronic relaxation of this interface with hybrid-DFT yielded a value for the electrostatic potential offset ΔV between the two bulk materials, from which the alignment of electronic states in the two materials could be determined, according to equations 1 and 2. In order to account for the opposing changes in electrostatic potentials of the materials upon formation of the average-lattice-constant supercell, the absolute volume deformation potentials (ADVPs) $a_v^i = \frac{dV^i}{d(ln(v))}$ were calculated for both materials using the method of Wei et al.[13,14] Within this method, an angular average is performed over the uniaxial deformation potentials $a_r^i = \frac{dV^i}{d(ln(r))}$, determined via a series of strained-homojunction supercell calculations, to yield a value for a_v^i.

$$\text{Valence Band Offset (VBO)} = \epsilon_{VBM}^A - \epsilon_{VBM}^B + \Delta V + a_v^A d(ln(v_A)) + a_v^B d(ln(v_B)) \quad (1)$$

$$\text{Conduction Band Offset (CBO)} = \epsilon_{CBM}^A - \epsilon_{CBM}^B + \Delta V + a_v^A d(ln(v_A)) + a_v^B d(ln(v_B)) \quad (2)$$

$$\text{CBO} = \text{VBO} + E_{g,A} - E_{g,B} + a_v^A d(lnV_A) + a_v^B d(lnV_B) \quad (3)$$

In the above equations, ϵ^i_{VBM} and ϵ^i_{CBM} are the eigenvalues (referenced to the average electrostatic potential) of the VBM and CBM for the ideal bulk material i, while $d(ln(v_i)) = \frac{\Delta v_i}{v_i}$ is the relative volume change between the equilibrium structure of i and the average-lattice-constant unit in the supercell. $E_{g,i}$ is the fundamental band gap of material i.

Convergence of the potential offset ΔV with respect to supercell size was verified by re-

peating the calculation with 80-atom (45 Å) and 120-atom cells (68 Å). While hybrid DFT (HSE06) was used in these supercell alignment calculations, in order to ensure accuracy and consistency, it is noted that both LDA and GGA standard DFT gave matching results in each case to within $0.02\,\mathrm{eV}$.

Results and Discussion

Crystal Structure

Structural relaxation of the experimentally-observed[15,16] elpasolite K_2NaAlF_6 crystal structure did not produce any alteration in symmetry for either $Cs_2AgSbBr_6$ or $Cs_2AgBiBr_6$. This structure, shown in figure 1, corresponds to the cubic $Fm\bar{3}m$ space group. Each of these ideal double perovskite structures is composed of a three-dimensional network of $[AgBr_6]^{5-}$ and $[SbBr_6]^{3-}$ or $[BiBr_6]^{3-}$ alternating corner-sharing octahedra. The Cs^+ cations are located in the interstitial cavities between octahedra, forming face-sharing $[CsBr_{12}]^{11-}$ cuboctahedra.
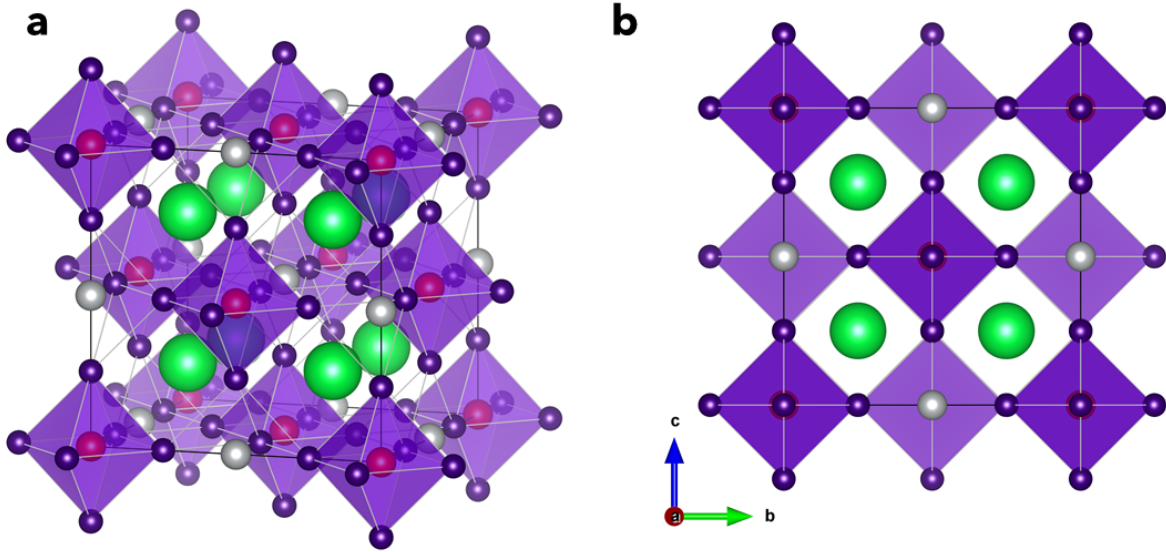

Figure 1: Equilibrium crystal structure of $Cs_2AgSbBr_6$ (and $Cs_2AgBiBr_6$)**(a)** and orientation along cubic lattice vector **(b)**. The $[SbBr_6]^{3-}$ ($[BiBr_6]^{3-}$) octahedra are coloured purple and the $[CsBr_{12}]^{11-}$ cuboctahedra are shown in green.

Within the $Fm\bar{3}m$ cubic space group, the atoms are located at the following Wyckoff po-

sitions: Cs: $8c(\frac{1}{4},\frac{1}{4},\frac{1}{4})$; Sb/Bi: $4a(0,0,0)$; Ag: $4b(\frac{1}{2},\frac{1}{2},\frac{1}{2})$; Br: $24e(x, 0, 0)$. In the perfectly symmetric case, $x = \frac{1}{2}$. Structural calculations reveal a slight off-centering of the bromine atoms from the perfectly-symmetric sites, as witnessed experimentally,[16,17] with $x = 0.2514$ for $Cs_2AgSbBr_6$ and $x = 0.2539$ for $Cs_2AgBiBr_6$. This is compared to an experimental value of $x = 0.25143(2)$ for $Cs_2AgBiBr_6$, measured at room-temperature with single-crystal XRD.[16] To the knowledge of the authors, no experimental values of x exist in literature for $Cs_2AgSbBr_6$,

Predicted lattice parameters at $T = 0\,\mathrm{K}$ for the conventional cubic unit cell are $11.082\,\mathrm{Å}$ for $Cs_2AgSbBr_6$ and $11.187\,\mathrm{Å}$ for $Cs_2AgBiBr_6$. As expected, $Cs_2AgSbBr_6$ exhibits a slightly smaller lattice parameter than $Cs_2AgBiBr_6$, due to the reduced ionic radius of Sb^{3+} $(76\,\mathrm{pm})$ relative to Bi^{3+} $(103\,\mathrm{pm})$.[18]

In all subsequent calculations, the ideal 'checkerboard' arrangement of Ag^+ and Sb^{3+}/Bi^{3+} sites was assumed, with zero structural disorder.

Electronic Structure

$Cs_2AgSbBr_6$

$Cs_2AgSbBr_6$ was found to have an indirect band gap, with the valence band maximum (VBM) located at $\mathbf{X} = (0.5, 0, 0.5)$ and the conduction band minimum (CBM) at $\mathbf{L} = (0.5, 0.5, 0.5)$. The fundamental band gap was initially calculated as $1.43\,\mathrm{eV}$ using the hybrid DFT functional HSE06, which decreased slightly to $1.37\,\mathrm{eV}$ upon the inclusion of spin-orbit coupling (SOC) effects. Electronic structure calculations by Wei et al. (HSE06+SOC) and Du et al. (HSE+SOC) yielded similar values of $1.46\,\mathrm{eV}$ and $1.67\,\mathrm{eV}$, respectively.[19,20] The direct band gap was calculated as $2.60\,\mathrm{eV}$, located at $\boldsymbol{b} = (0.5, 0.38, 0.62)$, along the high-symmetry reciprocal-space path Q from $\mathbf{L} = (0.5, 0.5, 0.5)$ to $\mathbf{W} = (0.5, 0.25, 0.75)$).
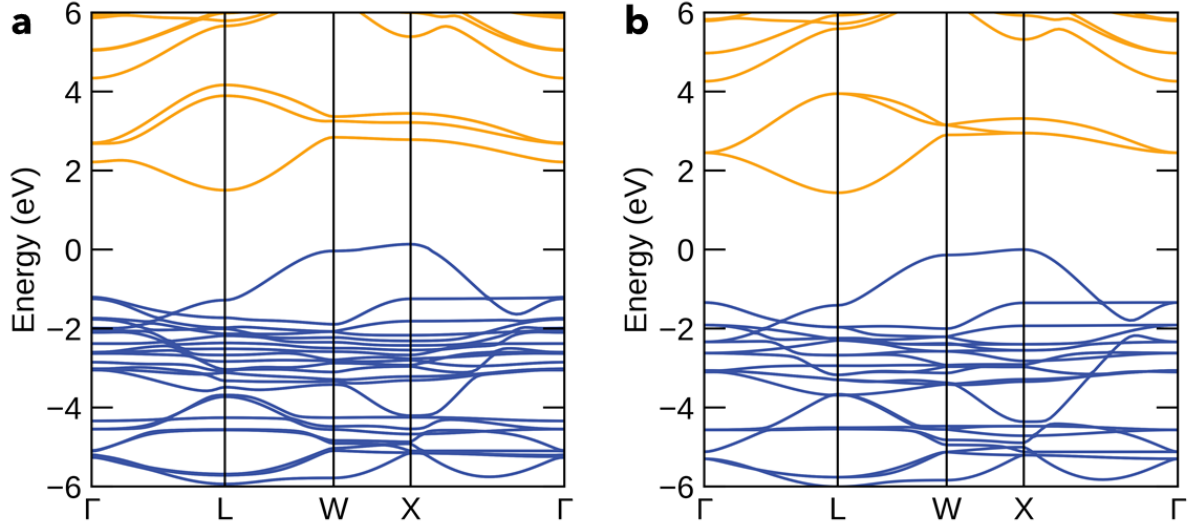
Figure 2: Calculated band structure of $Cs_2AgSbBr_6$ with **(a)** and without **(b)** spin-orbit coupling effects, illustrating the spin-orbit splitting of the conduction band. Valence band coloured blue, conduction band coloured orange. VBM set to 0 eV.

Spin-orbit splitting of the electronic states is primarily manifest in the conduction band, as demonstrated in figure 2. This is due to the strong Sb 5p orbital character of the conduction band, highlighted in figure 3, as the 5p orbitals split into $5p_{1/2}$ and $5p_{3/2}$ states.
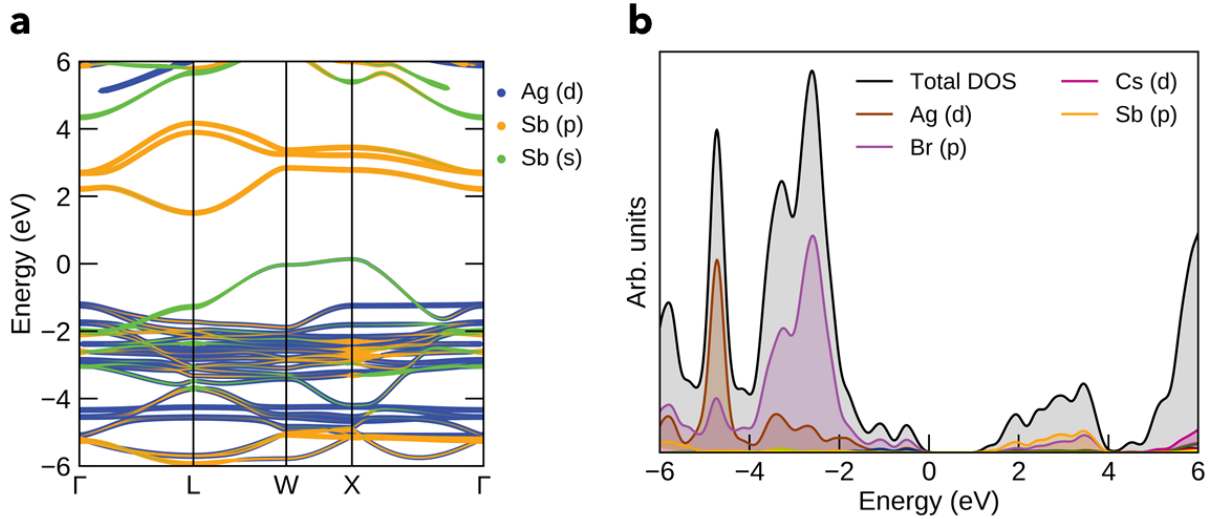

Figure 3: Projected band structure of $Cs_2AgSbBr_6$ **(a)** and electronic density of states **(b)**. VBM set to 0 eV.

Analysis of the electron band orbital character revealed that the conduction band states are

dominated by anti-bonding Sb 5p - Br 4p interactions, while the valence band states primarily arise from Br 4p, Ag 4d and Sb 5s orbital interactions. The Cs$^+$ cations act as spectator ions, as noted in literature,[21] with a relatively large nearest-neighbour-ion distance to Br$^-$ of 3.918 Å, compared to Sb-Br and Ag-Br bond lengths of 2.787 Å and 2.752 Å respectively.

Cs$_2$AgBiBr$_6$

Cs$_2$AgBiBr$_6$ was also found to have an indirect band gap, with the CBM and VBM located at the same high-symmetry k-points as Cs$_2$AgSbBr$_6$ (**L** and **X** respectively). The fundamental gap was initially calculated as 2.02 eV without spin-orbit interactions, which reduced significantly to 1.77 eV upon the inclusion of SOC effects.

HSE06+SOC electronic structure calculations by Savory et al. yielded a similar value of 1.79 eV,[22] with other levels of theory yielding values in the range 1.75-2.0 eV,[19,20,23–26] while experimental values in literature vary from 1.9-2.2 eV.[15,17,20,27–30]
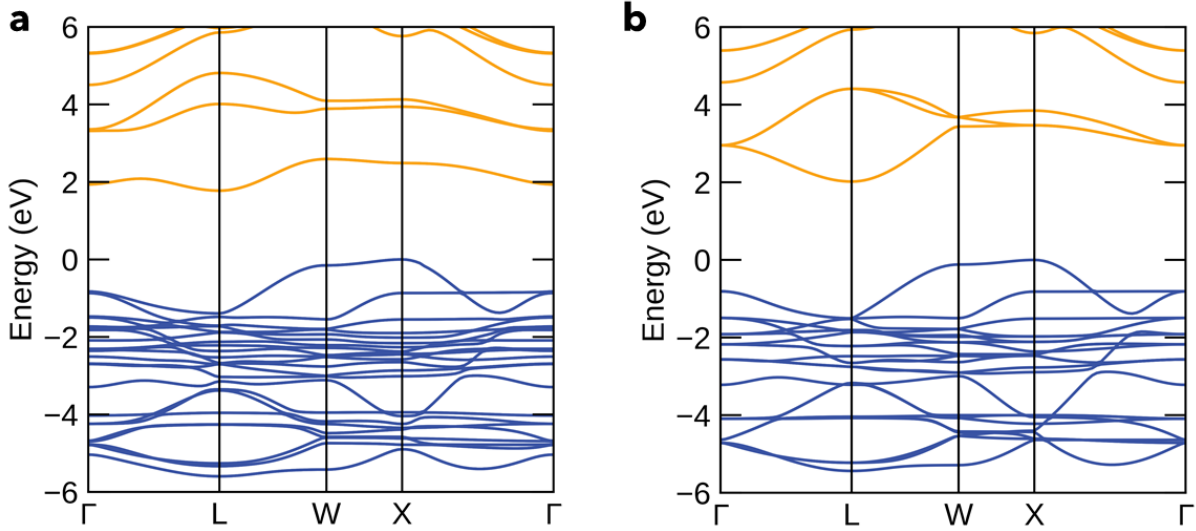

Figure 4: HSE06 band structure of Cs$_2$AgBiBr$_6$ calculated with (**a**) and without (**b**) spin-orbit coupling, demonstrating the significant spin-orbit splitting of the conduction band. Valence band coloured blue, conduction band coloured orange. VBM set to 0 eV.

The direct band gap was calculated as 2.49 eV, located at **X** = $(0.5, 0, 0.5)$. It is interesting to note that, despite a larger fundamental band gap, the direct gap of Cs$_2$AgBiBr$_6$ was

calculated to be smaller than that of $Cs_2AgSbBr_6$ (2.49 eV vs 2.60 eV), in addition to being located at a different point in k-space ($\mathbf{X} = (0.5, 0, 0.5)$ vs $\boldsymbol{b} = (0.5, 0.38, 0.62)$). From direct comparison of the band structures of both materials in figures 2a and 4a, it is evident that the differing reciprocal-space location of the direct gap is due to the stronger spin-orbit interactions of the Bi 6p orbitals in the $Cs_2AgBiBr_6$ CBM (see figure 5) relative to the Sb 5p orbital-dominated CBM in $Cs_2AgSbBr_6$.

The predicted values of the direct gaps compare favourably with reported experimental values; 2.51 eV,[17] 2.41 eV[27] for $Cs_2AgBiBr_6$ and 2.49 eV[19] for $Cs_2AgSbBr_6$.
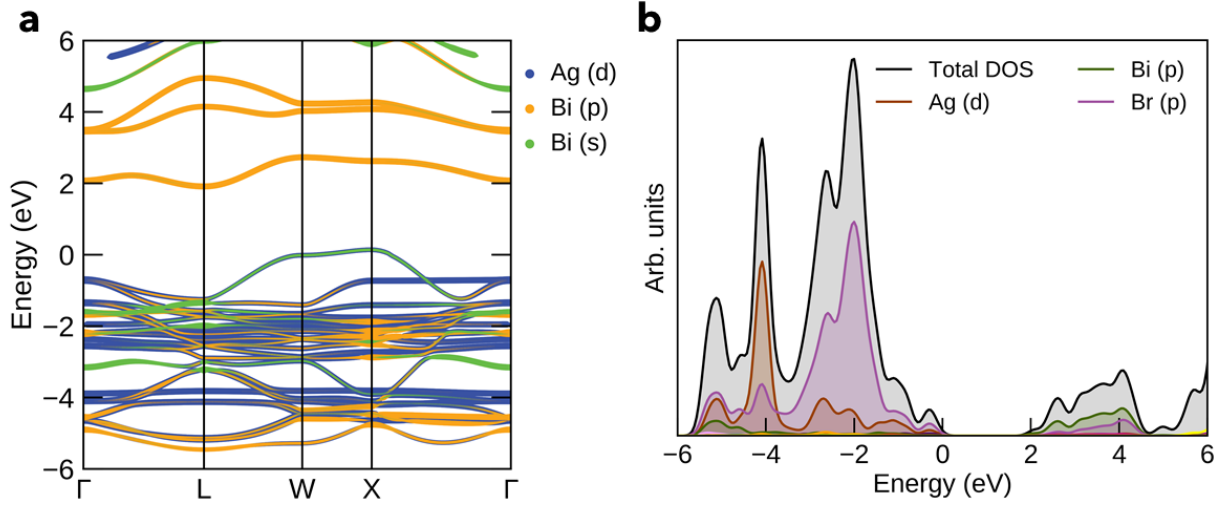

Figure 5: Projected band structure of $Cs_2AgBiBr_6$ **(a)** and electronic density of states **(b)**. VBM set to 0 eV.

As in the case of $Cs_2AgSbBr_6$, the conduction band states of $Cs_2AgBiBr_6$ are dominated by anti-bonding interactions between the trivalent pnictogen cation (Bi 6p) and halide anion (Br 4p) orbitals, while the valence band states primarily arise from Br 4p, Ag 4d and Bi 6s orbital interactions. As with $Cs_2AgSbBr_6$, the Cs^+ cations act as spectator ions, with a large nearest-neighbour-ion distance to Br^- of 3.955 Å, compared to Bi-Br and Ag-Br bond lengths of 2.841 Å and 2.752 Å respectively. In both cases, the calculated orbital projections of the VBM and CBM states agree with other theoretical investigations of these materials.[20,22,31]

The charge carrier effective mass values for both materials, calculated using non-parabolic fitting of the band structures, are tabulated below.

Table 1: Calculated effective mass values for $Cs_2AgSbBr_6$ and $Cs_2AgBiBr_6$ in units of electron mass.

Material	$m_h^{\Gamma-X}$	m_h^{X-W}	m_e^{W-L}	$m_e^{L-\Gamma}$
$Cs_2AgSbBr_6$	0.15	0.62	0.26	0.32
$Cs_2AgBiBr_6$	0.18	0.61	0.31	0.45

Electron Band Alignment

The 'natural' band offset of the two double perovskite materials was determined using equation 3, and is shown in figure 6. $a_v^{Cs_2AgSbBr_6} = 7.63\,V$ and $a_v^{Cs_2AgBiBr_6} = 7.41\,V$ were the calculated deformation potentials. Our investigations indicate a 'staggered gap' (type II) heterojunction alignment, with a valence band offset (VBO) of $0.75\,eV$ and a conduction band offset (CBO) of $0.34\,eV$ ($Cs_2AgSbBr_6$ above $Cs_2AgBiBr_6$ in both cases).

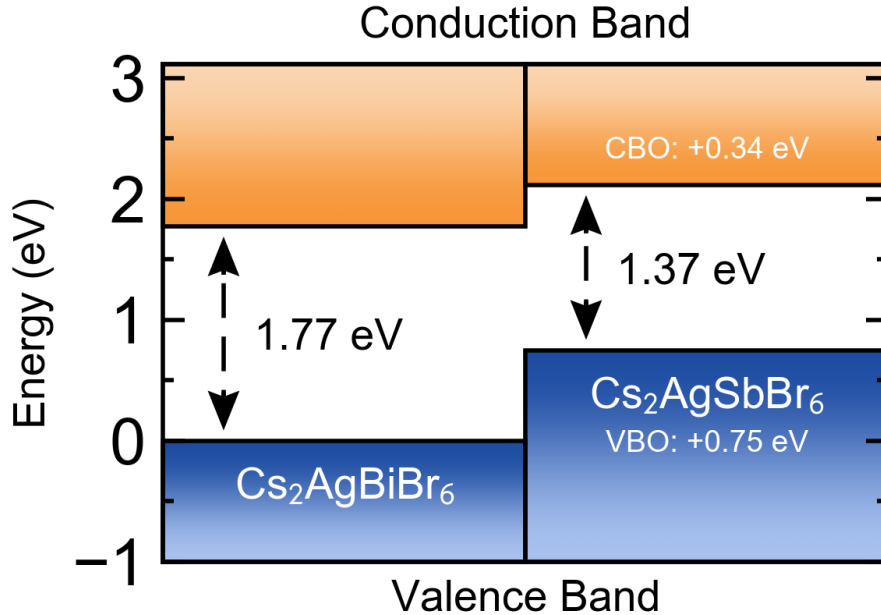**Figure 6:** Electron band alignment of $Cs_2AgBiBr_6$ and $Cs_2AgSbBr_6$. CBO = Conduction Band Offset, VBO = Valence Band Offset.

Such band alignment suggests the possibility of significant band gap bowing in a mixed-metal random alloy of the two materials, as a consequence of an aperiodic crystal potential.[32] If a perfectly-ordered crystal were obtained upon alloying, with a homogeneous distribution of Sb and Bi in the alloy compositional ratio, one would expect approximately linear shifts in the CBM and VBM, with only a small degree of band gap bowing. However, in the more realistic picture of a random alloy, 'imperfect' mixing of electronic states can occur, with crystal regions of greater Sb proportion than the overall alloy ratio (yielding a higher VBM) and vice versa (yielding a lower CBM). Thus, the combination of a type II staggered gap alignment and an aperiodic distribution of bismuth and antimony in the alloy material can lead to a band gap which is in fact smaller than the fundamental gap of either pure material.

It is typically expected from (non-relativistic) molecular orbital theory that atomic substitution with heavier members from a group in the periodic table provides higher-energy, more diffuse valence orbitals, leading to increased orbital overlap, greater electron band dispersion and consequently a smaller separation between the valence band and conduction band states.[31,33,34] However, the reduced band gap of $Cs_2AgSbBr_6$ relative to $Cs_2AgBiBr_6$ is an interesting contradiction to the usual trend of decreasing band gap with increasing atomic radius for elements in the same periodic group.

From figure 6, the reduction in band gap upon substitution of Bi^{3+} with Sb^{3+} in $Cs_2AgBiBr_6$ can be attributed to the higher energy VBM of the antimony-containing perovskite. This can be understood through consideration of the orbital character of the electron band extrema. As mentioned earlier, and shown in figure 8, there is significant cation s orbital character in the electronic density of states at the VBM. Typically, the energies of valence electrons becomes less negative as one moves down a group in the periodic table, corresponding to a decrease in ionisation energies. However, for Bi^{3+} and Sb^{3+}, this is not the case, with the Bi^{3+} $6s^2$ lone pair being lower in energy than the Sb^{3+} $5s^2$ lone pair.[35] This is a result of the relativistic contraction of the Bi 6s orbital, due to its large atomic number, resulting

in a more localised, lower-energy valence s orbital, compared to Sb 5s.[36] Consequently, the more-diffuse, higher-energy Sb $5s^2$ lone-pair has a stronger interaction with the Ag 4d and Br 4p orbitals, due to a reduced energy separation of the bonding orbitals. This produces both greater dispersion in the valence band and a higher energy VBM, as shown schematically in figure 7. The importance of this cation s - anion p interaction in determining the valence band position in halide double perovskites has been previously noted.[22,37] Indeed, the similar cation (Pb^{3+}) s - anion (I^-) p anti-bonding interactions that are partially attributed to the outstanding photovoltaic properties of lead-based perovskites.[38]
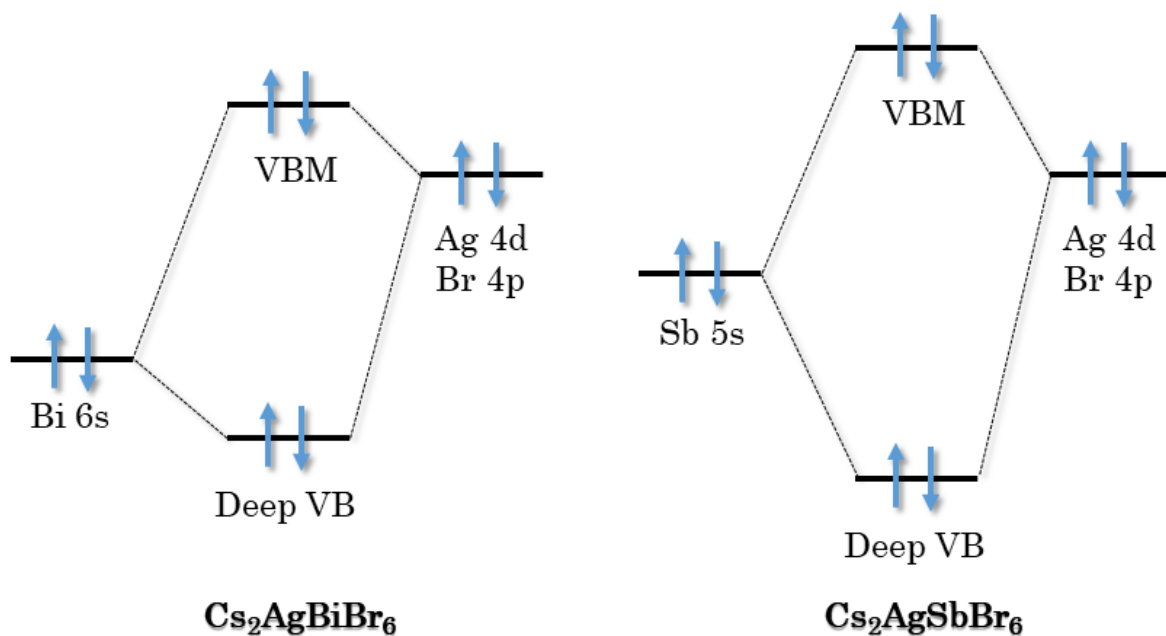

Figure 7: Schematic molecular orbital diagram demonstrating the effect of cationic lone-pair interactions on the VBM position.

There are multiple sources of evidence for this effect. Firstly, it is apparent from the VBM density of states in figure 8 that there is a greater degree of Sb 5s character at the VBM of $Cs_2AgSbBr_6$ than Bi 6s in the VBM of $Cs_2AgSbBr_6$.

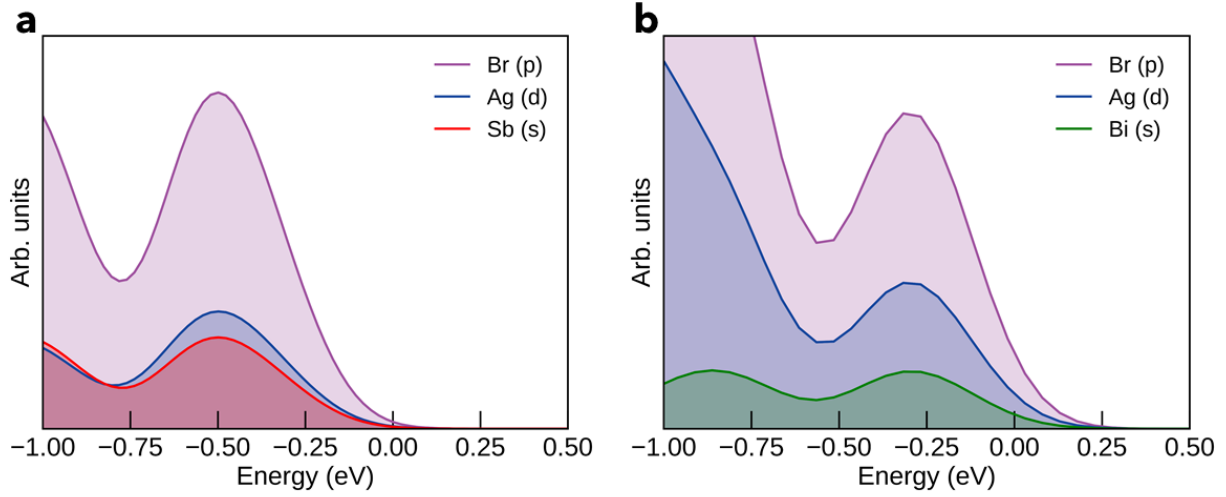**Figure 8:** Electronic density of states of $Cs_2AgBiBr_6$ and $Cs_2AgSbBr_6$ near the VBM. VBM set to 0 eV.

Another point of evidence for this effect is the greater valence band width in $Cs_2AgSbBr_6$ (figure 3a) of $\sim 1.64\,\text{eV}$ compared to $\sim 1.38\,\text{eV}$ in $Cs_2AgBiBr_6$ (figure 5a). Moreover, a greater energy separation between the VBM and the lowest energy pnictogen s states is witnessed for $Cs_2AgSbBr_6$ (corresponding to the 'deep VB' states in figure 7), a predicted consequence of stronger orbital interactions.

It is noted that the increased valence band width in $Cs_2AgSbBr_6$ is likely aided by the reduced cation-bromine nearest-neighbour distances in this material (2.787 Å for Sb-Br vs 2.841 Å for Bi-Br).

A previous theoretical investigation of these materials by Volonakis et al. also predicted a reduction in band gap upon substitution of bismuth with antimony in $Cs_2AgBiBr_6$.[31] However, in this case, the authors attributed the decrease in band gap to a decrease in energy of the pnictogen p states, thus lowering the energy of the conduction band minimum. Our results contradict this hypothesis. While the first ionisation energy of Sb is indeed larger than than of Bi, the third ionisation energy (corresponding to the removal of a p electron from Sb^{2+}/Bi^{2+}) is in fact 0.3 eV lower for Sb than for Bi,[35] indicating *higher* energy p

states. When the pnictogen elements are in the +3 oxidation state, as is the case in these materials, the third ionisation energy gives a better estimate for the energy of the unoccupied p orbitals. Hence we argue that, in the +3 charge state, the Sb valence p orbital states are in fact higher in energy than those of Bi, suggesting a higher energy CBM for $Cs_2AgSbBr_6$, as witnessed in our investigations.

Another theoretical study of these materials, by Du et al, also predicted the reduction in band gap from $Cs_2AgBiBr_6$ to $Cs_2AgSbBr_6$.[20] In agreement with our findings, a positive VBO of $Cs_2AgSbBr_6$ relative to $Cs_2AgBiBr_6$ was predicted, with a calculated value of 0.29 eV. However, the CBO was calculated as -0.04 eV, a divergence from our predicted value of 0.34 eV. However, in this case, band alignment was performed using the Cs 5s levels, which is not a reliable reference. This is due to the fact that orbital energies will vary significantly with changes in chemical environment,[39] as witnessed in our investigations.

Optical Properties

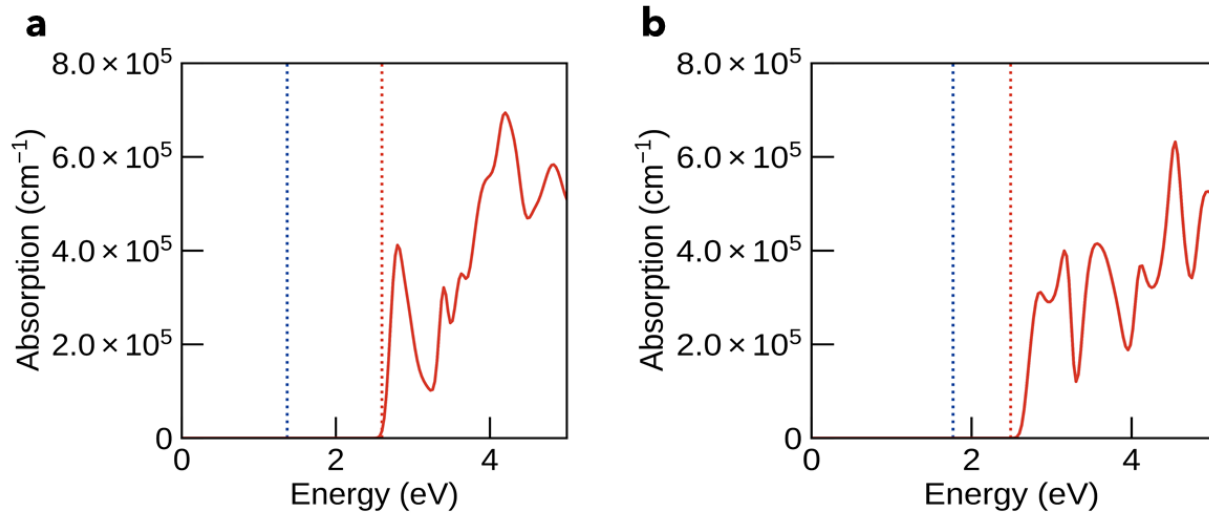The optical absorption was calculated for both materials, as shown in figures 9 and 10.

Figure 9: Optical absorption plots of $Cs_2AgSbBr_6$ **(a)** and $Cs_2AgBiBr_6$ **(b)**. Fundamental (indirect) and optical (direct) gaps indicated by dashed blue and red lines, respectively.
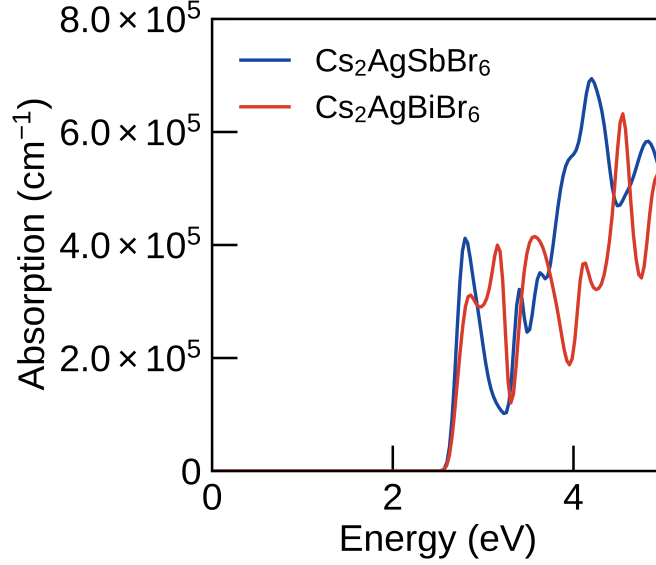
Figure 10: Superimposed optical absorption plots of $Cs_2AgSbBr_6$ (**blue**) and $Cs_2AgBiBr_6$ (**red**).

For both materials, the lowest direct electronic gap corresponds to a symmetry-allowed transition from the valence band to the conduction band. Thus, the direct gap is equivalent to the optical gap of each material. The calculated dielectric constants, optical exciton binding energies $E_{ex,opt}$ and spectroscopic limited maximum efficiencies (SLME)[40] η_{SLME} are provided in table 2.

Table 2: Calculated dielectric constants, optical exciton binding energies $E_{ex,opt}$ and spectroscopic limited maximum efficiencies (SLME)[40] η_{SLME} (for 1 μm thick absorber material) of $Cs_2AgSbBr_6$ and $Cs_2AgBiBr_6$.

Material	ϵ_{Ionic}	ϵ_∞	$\epsilon_0 = \epsilon_{ionic} + \epsilon_\infty$	$E_{ex,opt}$	η_{SLME}
$Cs_2AgSbBr_6$	8.87	4.82	13.69	124 meV	4.49%
$Cs_2AgBiBr_6$	8.16	4.60	12.76	167 meV	6.06%

Filip et al. calculated a similar value of 5.8 for the high-frequency dielectric constant (ϵ_∞) of $Cs_2AgBiBr_6$,[17] using the random-phase-approximation (RPA), while Steele et al. reported values of 5.42 and 16.73 for ϵ_∞ and ϵ_0 ($Cs_2AgBiBr_6$).[27] However, in the latter case, density functional perturbation theory (DFPT) was used for the calculation of ϵ_∞, which is well-known to overestimate values for ϵ_∞ as a consequence of the band-gap underestimation in

DFT.[41]

It is proposed that the larger dielectric constant of $Cs_2AgSbBr_6$ can be attributed to a smaller band gap and lattice constant (and thus a larger atomic density).

The spectroscopic limited maximum efficiency η_{SLME} is a metric proposed by Yu and Zunger that includes the strength of optical absorption and the nature of the band gap in the overall theoretical efficiency of a photovoltaic absorber material.[40]

The calculated values of η_{SLME} are significantly reduced from the Shockley-Quiesser limit efficiencies of $\sim 11\%$. This is a direct consequence of the fact that both materials possess fundamental (indirect) gaps which are significantly smaller than the optical (direct) gaps, thereby incurring substantial non-radiative losses in efficiency as charge carriers relax to the band edges before extraction.

From the calculated values for the effective masses (Table 1) and dielectric constants (Table 2), the optical exciton binding energies were determined under the effective mass approximation:[42]

$$\text{E}_{ex,opt} \; = \; (\frac{m^*}{m_0\epsilon_\infty^2})\text{R}_H \tag{4}$$

where $m^* = \frac{m_e m_h}{m_e+m_h}$ is the reduced effective mass, m_0 is the electronic mass, R_H is the Rydberg constant and ϵ_∞ is the optical dielectric constant as before.

Acknowledgements

References

(1) Kresse, G.; Hafner, J. Ab initio molecular dynamics for liquid metals. *Physical Review B* **1993**, *47*, 558–561.

(2) Kresse, G.; Hafner, J. Ab initio molecular-dynamics simulation of the liquid-metalamorphous- semiconductor transition in germanium. *Physical Review B* **1994**, *49*, 14251–14269.

(3) Kresse, G.; Furthmüller, J. Efficiency of ab-initio total energy calculations for metals and semiconductors using a plane-wave basis set. *Computational Materials Science* **1996**, *6*, 15–50.

(4) Kresse, G.; Furthmüller, J. Efficient iterative schemes for ab initio total-energy calculations using a plane-wave basis set. *Physical Review B - Condensed Matter and Materials Physics* **1996**, *54*, 11169–11186.

(5) Perdew, J. P.; Ruzsinszky, A.; Csonka, G. I.; Vydrov, O. A.; Scuseria, G. E.; Constantin, L. A.; Zhou, X.; Burke, K. Restoring the density-gradient expansion for exchange in solids and surfaces. *Physical Review Letters* **2008**, *100*.

(6) Krukau, A. V.; Vydrov, O. A.; Izmaylov, A. F.; Scuseria, G. E. Influence of the exchange screening parameter on the performance of screened hybrid functionals. *Journal of Chemical Physics* **2006**, *125*.

(7) Perdew, J. P.; Burke, K.; Ernzerhof, M. Generalized gradient approximation made simple. *Physical Review Letters* **1996**, *77*, 3865–3868.

(8) Blöchl, P. E. Projector augmented-wave method. *Physical Review B* **1994**, *50*, 17953–17979.

(9) Gajdoš, M.; Hummer, K.; Kresse, G.; Furthmüller, J.; Bechstedt, F. Linear optical properties in the projector-augmented wave methodology. *Physical Review B - Condensed Matter and Materials Physics* **2006**, *73*.

(10) Whalley, L. D. effmass: An effective mass package Software ● Review ● Repository ● Archive. **2018**,

(11) Ganose, A. M.; Jackson, A. J.; Scanlon, D. O. sumo: Command-line tools for plotting and analysis of periodic ab initio calculations Software ● Review ● Repository ● Archive. **2018**,

(12) Butler, K. T.; Hendon, C. H.; Walsh, A. Electronic Chemical Potentials of Porous Metal–Organic Frameworks. *Journal of the American Chemical Society* **2014**, *136*, 2703–2706.

(13) Li, Y.-H.; Gong, X. G.; Wei, S.-H. Ab initio calculation of hydrostatic absolute deformation potential of semiconductors. *Appl. Phys. Lett* **2006**, *88*, 42104.

(14) Von Der Lage, F. C.; Bethe, H. A. *A Method for Obtaining Electronic Eigenfunctions and Eigenvalues in Solids with An Application to Sodium**.

(15) Slavney, A. H.; Hu, T.; Lindenberg, A. M.; Karunadasa, H. I. A Bismuth-Halide Double Perovskite with Long Carrier Recombination Lifetime for Photovoltaic Applications. *Journal of the American Chemical Society* **2016**, *138*, 2138–2141.

(16) Schade, L.; Wright, A. D.; Johnson, R. D.; Dollmann, M.; Wenger, B.; Nayak, P. K.; Prabhakaran, D.; Herz, L. M.; Nicholas, R.; Snaith, H. J.; Radaelli, P. G. Structural and Optical Properties of Cs 2 AgBiBr 6 Double Perovskite. *Cite This: ACS Energy Lett* **2019**, *4*, 305.

(17) Filip, M. R.; Hillman, S.; Haghighirad, A. A.; Snaith, H. J.; Giustino, F. Band Gaps of

the Lead-Free Halide Double Perovskites Cs2BiAgCl6 and Cs2BiAgBr6 from Theory and Experiment. *Journal of Physical Chemistry Letters* **2016**, *7*, 2579–2585.

(18) Shannon, R. D. Revised effective ionic radii and systematic studies of interatomic distances in halides and chalcogenides. *Acta Crystallographica Section A* **1976**, *32*, 751–767.

(19) Wei, F.; Deng, Z.; Sun, S.; Hartono, N. T. P.; Seng, H. L.; Buonassisi, T.; Bristowe, P. D.; Cheetham, A. K. Enhanced visible light absorption for lead-free double perovskite Cs 2 AgSbBr 6. *Chemical Communications* **2019**, *55*, 3721–3724.

(20) Du, K.-z.; Meng, W.; Wang, X.; Yan, Y.; Mitzi, D. B. Bandgap Engineering of Lead-Free Double Perovskite Cs ¡sub¿2¡/sub¿ AgBiBr ¡sub¿6¡/sub¿ through Trivalent Metal Alloying. *Angewandte Chemie International Edition* **2017**, *56*, 8158–8162.

(21) Stamplecoskie, K. G.; Manser, J. S.; Kamat, P. V. Dual nature of the excited state in organic-inorganic lead halide perovskites. *Energy and Environmental Science* **2015**, *8*, 208–215.

(22) Savory, C. N.; Walsh, A.; Scanlon, D. O. Can Pb-Free Halide Double Perovskites Support High-Efficiency Solar Cells? *ACS Energy Letters* **2016**, *1*, 949–955.

(23) Guechi, N.; Bouhemadou, A.; Bin-omran, S.; Bourzami, A.; Louail, L.; Abbas Setif, F. Elastic, Optoelectronic and Thermoelectric Properties of the Lead-Free Halide Semiconductors Cs2AgBiX 6 (X = Cl, Br): Ab Initio Investigation. *University Ferhat Abbas Setif* **1900**, *1*.

(24) Xiao, Z.; Meng, W.; Wang, J.; Yan, Y. Thermodynamic Stability and Defect Chemistry of Bismuth-Based Lead-Free Double Perovskites. *ChemSusChem* **2016**, *9*, 2628–2633.

(25) Yang, J.; Zhang, P.; Wei, S.-H. Band Structure Engineering of Cs ¡sub¿2¡/sub¿ AgBiBr

$_6$ Perovskite through Order–Disordered Transition: A First-Principle Study. *The Journal of Physical Chemistry Letters* **2018**, *9*, 31–35.

(26) Haque, E.; Hossain, M. A. Origin of ultra-low lattice thermal conductivity in Cs 2 BiAgX 6 (X=Cl, Br) and its impact on thermoelectric performance. *Journal of Alloys and Compounds* **2018**, *748*, 63–72.

(27) Steele, J. A.; Puech, P.; Keshavarz, M.; Yang, R.; Banerjee, S.; Debroye, E.; Kim, C. W.; Yuan, H.; Heo, N. H.; Vanacken, J.; Walsh, A.; Hofkens, J.; Roeffaers, M. B. Giant electron-phonon coupling and deep conduction band resonance in metal halide double perovskite. *ACS Nano* **2018**, *12*, 8081–8090.

(28) Bartesaghi, D.; Slavney, A. H.; Gélvez-Rueda, M. C.; Connor, B. A.; Grozema, F. C.; Karunadasa, H. I.; Savenije, T. J. Charge Carrier Dynamics in Cs $_2$ AgBiBr $_6$ Double Perovskite. *The Journal of Physical Chemistry C* **2018**, *122*, 4809–4816.

(29) Lozhkina, O. A.; Murashkina, A. A.; Elizarov, M. S.; Shilovskikh, V. V.; Zolotarev, A. A.; Kapitonov, Y. V.; Kevorkyants, R.; Emeline, A. V.; Miyasaka, T. Microstructural analysis and optical properties of the halide double perovskite Cs2BiAgBr6 single crystals. *Chemical Physics Letters* **2018**, *694*, 18–22.

(30) McClure, E. T.; Ball, M. R.; Windl, W.; Woodward, P. M. Cs $_2$ AgBiX $_6$ (X = Br, Cl): New Visible Light Absorbing, Lead-Free Halide Perovskite Semiconductors. *Chemistry of Materials* **2016**, *28*, 1348–1354.

(31) Volonakis, G.; Filip, M. R.; Haghighirad, A. A.; Sakai, N.; Wenger, B.; Snaith, H. J.; Giustino, F. Lead-Free Halide Double Perovskites via Heterovalent Substitution of Noble Metals. *Journal of Physical Chemistry Letters* **2016**, *7*, 1254–1259.

(32) Niedermeier, C. A.; Råsander, M.; Rhode, S.; Kachkanov, V.; Zou, B.; Alford, N.; Moram, M. A. Band gap bowing in Nix Mg1-x O. *Scientific Reports* **2016**, *6*, 1–9.

(33) Tang, L. C.; Chang, C. S.; Huang, J. Y. Electronic structure and optical properties of rhombohedral CsGeI3 crystal. *Journal of Physics Condensed Matter* **2000**, *12*, 9129–9143.

(34) Hao, F.; Stoumpos, C. C.; Cao, D. H.; Chang, R. P.; Kanatzidis, M. G. Lead-free solid-state organic-inorganic halide perovskite solar cells. *Nature Photonics* **2014**, *8*, 489–494.

(35) Lide, D. R. *CRC Handbook of Chemistry and Physics*, 84th ed.; CRC Press: Florida, 2003; Chapter 10: Atomic.

(36) Pyykkö, P. Relativistic Effects in Structural Chemistry. *Chemical Reviews* **1988**, *88*, 563–594.

(37) Tran, T. T.; Panella, J. R.; Chamorro, J. R.; Morey, J. R.; McQueen, T. M. Designing indirect-direct bandgap transitions in double perovskites. *Materials Horizons* **2017**, *4*, 688–693.

(38) Yin, W. J.; Shi, T.; Yan, Y. Unique properties of halide perovskites as possible origins of the superior solar cell performance. *Advanced Materials* **2014**, *26*, 4653–4658.

(39) Li, Y. H.; Walsh, A.; Chen, S.; Yin, W. J.; Yang, J. H.; Li, J.; Da Silva, J. L.; Gong, X. G.; Wei, S. H. Revised ab initio natural band offsets of all group IV, II-VI, and III-V semiconductors. *Applied Physics Letters* **2009**, *94*.

(40) Yu, L.; Zunger, A. Identification of potential photovoltaic absorbers based on first-principles spectroscopic screening of materials. *Physical Review Letters* **2012**, *108*, 068701.

(41) Petousis, I.; Chen, W.; Hautier, G.; Graf, T.; Schladt, T. D.; Persson, K. A.; Prinz, F. B. Benchmarking density functional perturbation theory to enable high-throughput screen-

ing of materials for dielectric constant and refractive index. *PHYSICAL REVIEW B* **2016**, *93*, 115151.

(42) Böer, K. W.; Pohl, U.; Böer, K. W.; Pohl, U. W. *Semiconductor Physics*; Springer International Publishing, 2015; pp 1–41.